DOI: 10.1002/ejic.201000372

Synthesis, Structure, and Sensor Properties of Vanadium Pentoxide Nanorods

Anastasia V. Grigorieva,*[a] Siranuysh M. Badalyan,[b] Eugene A. Goodilin,[a,b] Marina N. Rumyantseva,[b] Alexander M. Gaskov,[b] Alexander Birkner,[c] and Yuri D. Tretyakov[a,b]

Keywords: Vanadium oxides / Nanostructures / Hydrothermal synthesis / Resistive-type gas sensor

Vanadium oxide nanorods were prepared by a hydrothermal route and then tested as a transducer for a resistive-type gas sensor. The importance of control of pH and pressure during the synthesis of 1D crystals of vanadium oxide was demonstrated for the V_2O_5/ethanol mixture, which served as a precursor. As a gas sensor element, the nanorods demonstrated a stable response to triethylamine and weak sensor response to carbon monoxide with a short response time (as low as 32 s).

1. Introduction

Crystalline needles of transition metal oxides deserve attention because of their stability under ambient conditions and their unusual physical and chemical properties.[1] Vanadium oxides are well-known semiconductor catalysts[2] and electrochromic materials,[3] as well as sensor[4] and cathode materials for lithium-ion batteries.[5] New nanostructures based on vanadium oxides, such as nanotubes,[6] nanobelts,[7] nanowires, and nanorods[8] have been insufficiently studied. These materials differ from traditional ceramics by a significant influence of surface characteristics on their functional properties. In this work vanadium pentoxide nanorods have been synthesized and analyzed with respect to their sensor properties.

The coordination chemistry of vanadium results in the ability of some vanadium oxides to demonstrate a high response and selective interaction with some gases.[9] Indeed, a number of chemical sensors, based on mixed-valence vanadium oxides, have been already successfully produced and tested,[6] including sensors of alcohols,[8,10,11] carbon monoxide,[8] nitrogen dioxide,[8] acetylacetone,[8] ammonia,[9] and humidity.[11] 1D-Nanostructured vanadium oxides are of interest as a way to develop sensors based on a single particle. Recently, nanobelts of vanadium(IV–V) oxides were reported as promising materials for ethanol sensors,[7] nanofibers of V_2O_5 were found to be promising as an ammonia sensor material;[12] nanofibers of vanadium pentoxide were also reported to be sensitive to alcohols (methanol, ethanol, and butanol).[13] Some synthetic techniques for the preparation of vanadium oxide nanorods have been described in ref.[14]; however, their mechanisms of formation and sensor properties have not yet been sufficiently examined.

[a] Materials Science Department, Lomonosov Moscow State University,
Leninskie gory, Moscow 119992, Russian Federation
Fax: +7-495-939-0998
E-mail: anastasia@inorg.chem.msu.ru
[b] Chemistry Department, Lomonosov Moscow State University, Leninskie gory, Moscow 119992, Russia
[c] Faculty of Physical Chemistry 1, Ruhr-Universität Bochum, Universitätsstraße 150, 44780 Bochum, Germany

2. Results and Discussion

2.1. Characterization of Products

The microstructure of the product is shown in Figure 1 and gives evidence for the formation of nanowires or nanorods, which are about 50 nm thick and 10 μm long, with the presence of a negligible amount of particles with a different morphology (Figure 1a). The sample appears to be of a single phase and monocrystalline (Figure 1b). The specific surface area of the sample, calculated by using the Brunauer–Emmett–Teller (BET) method, is 28 ± 3 m^2/g, which is typical for inorganic nanorods and nanoribbons.

The uneven edges of the particles (Figure 1a) indicate that the shape of the particles is closer to that of nanobelts and nanoribbons rather than to acicular needle-like crystals (Figure 1b). The monocrystallinity of the nanorods was confirmed by electron diffraction on individual particles and also from the striped patterns observed in TEM images. The interlayer distances (parallel to the growth axis) found in the images correspond to doubled *b* or *c* parameters. The typical electron diffraction of an individual nanorod, measured perpendicular to the layers, is shown in Figure 1c. The diffraction image could be interpreted as having (001) plane reflections of V_2O_5 with parameters of the unit cell $a = 11.4(5)$ and $b = 3.5(1)$ Å.

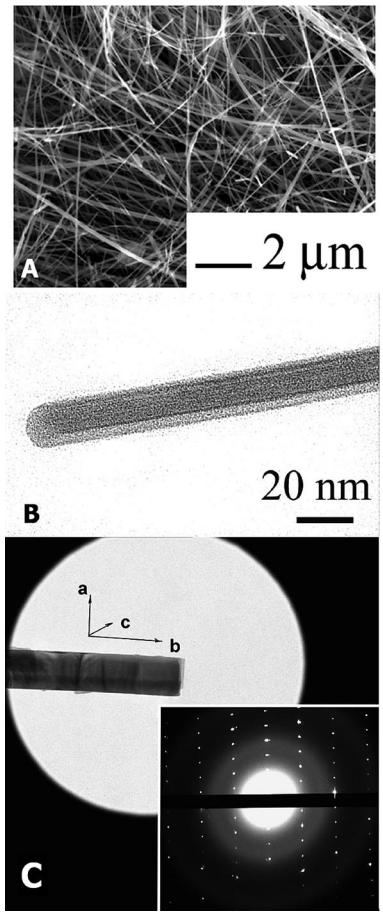

Figure 1. Microstructure and crystallinity of vanadium oxide nanorods synthesized in an H_2O/C_2H_5OH environment: SEM (a) and TEM (b) micrographs with electron diffraction image (c) of an individual nanorod. Indexing gives V–O layers perpendicular to the <010> direction.

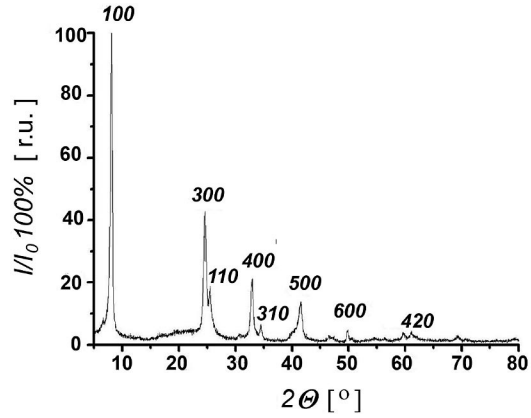

Figure 2. XRD data for $H_xV_2O_5{\cdot}nH_2O$ vanadium oxide nanorods. Indexing is given according to V_2O_5 (PDF2 database file number 41-1426) and $H_xV_2O_5$ (PDF2 database file number 45-429).

The XRD data given in Figure 2 confirm that the sample consists of a single phase with a perfect *h*00 texture. Most of the XRD reflections correspond to an *h*00 series for hydrated V_2O_5 with orthorhombic syngony (PDF2 database file number 41-1426). According to the electron diffraction and XRD data the structure of the nanorods is of orthorhombic syngony and is built of {UD} chains of square pyramids as described in ref.[15]

The product was greenish-yellow in color, which indicates the presence of a reduced vanadium V^{4+} species. FTIR spectra of the material (Figure 3a) reveal an absorption at 995 cm^{-1} that corresponds to the ν(V=O) stretching mode, typical for vanadium pentoxide. Two shoulders at about 490 and 668 cm^{-1} can be interpreted as ν(V–O) stretching modes. Two types of V–O bonds are present in the sample, which are V–OH and V–O–V groups, respectively. The acidity of the V–OH centers seems to be suitable for interaction with gaseous oxidizing agents such as oxygen and nitrogen dioxide. The FTIR spectrum of the nanorods differs significantly from the IR spectrum of the $V_4O_{10}^{\delta-}$ anion[15] but correlates with the spectrum of vanadium pentoxide.

The X-ray photoelectron spectra (XPS) for V 2p and O 1s cores are shown in Figure 3b and c. The O 1s core spectrum shows three types of oxygen atoms at the nanorod surfaces. The peaks at 532.7(1) and 531.1(1) eV originated from adsorbed water molecules and hydroxy groups, respectively. The peak at 529.8(1) eV belongs to lattice oxygen atoms. In the spectrum of the vanadium core the maxima are located at 524.5(2) and 517.0(2) eV. Such values correspond to neither V_2O_5 nor VO_2 and reflect a mixed-valence state of the vanadium at the surface.[16] In the case of our product, we observed two pairs of V $2p_{1/2}$ and V $2p_{3/2}$ peaks, which correspond to two oxidation states of vanadium on the surface of the particles. The positions of the V $2p_{1/2}$ and V $2p_{3/2}$ peaks were determined as 524.9(2) and 517.5(2) eV for V^{5+} and 524.0(2) and 516.2(2) eV for V^{4+}. The surface of the $V_2O_5{\cdot}H_2O$ nanorods prepared was partially reduced, which explains the greenish tint of the product. According to XPS spectra the proportion of V^{4+} in the sample does not exceed 10%.

The experimental data demonstrate the similarity of the structure of vanadium oxide nanorods to the structure of the hydrated form of vanadium pentoxide and vanadium pentoxide gels $V_2O_5{\cdot}nH_2O$ where the proportion of V^{4+} can reach 20% without change to the structure.[17] According to thermogravimetric/differential thermal analysis and XRD data $n \approx 0.5$. Another opinion of the structure of vanadia gels and nanorods is given in ref.[18] where the authors describe the materials as monoclinic δ-$H_xV_4O_{10}{\cdot}nH_2O$ bronzes. The structure of the nanorods obtained here is similar to orthorhombic V_2O_5 and the chemical composition is also close to both vanadia gels and vanadium bronzes; thus, we assume the nanorods to be δ-$H_xV_2O_5{\cdot}nH_2O$ bronzes.

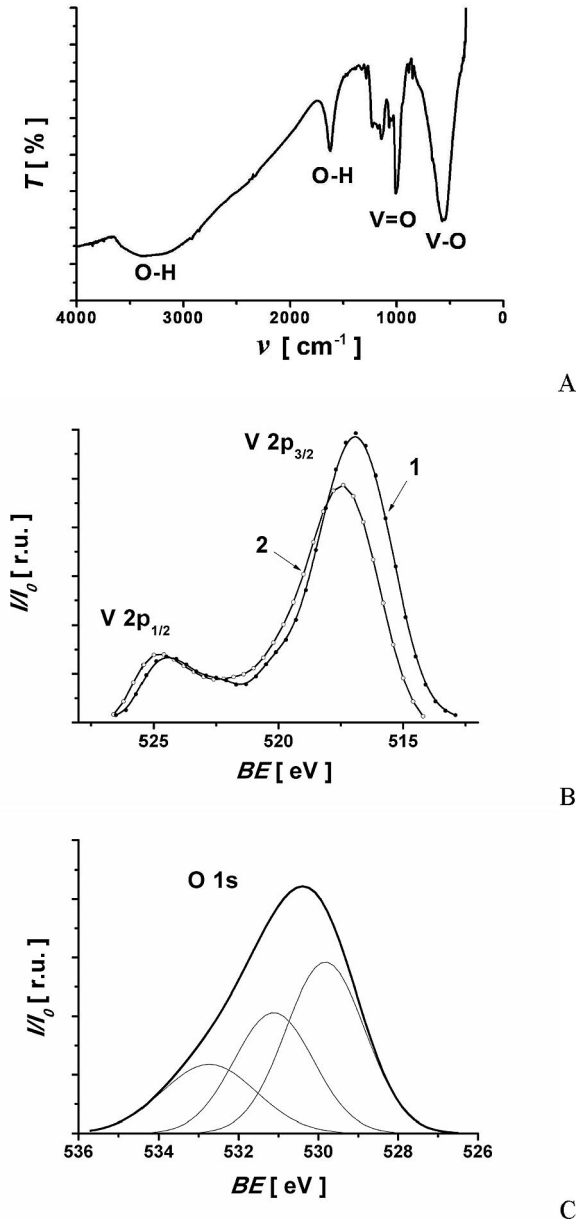

Figure 3. Vanadium oxidation state analysis for vanadium oxide nanorods: FTIR data (a) and XPS spectra for V 2p core (b) and O 1s peaks (c).

A general view of the nanorod chip assembly is shown in Figure 4a. The thick film of vanadia nanorods demonstrates the negative slope of $R(T)/(R_0 - 1/T)$ dependence in the Arrhenius plot, revealing the n-type conductivity character in the whole working range (room temp. to 200 °C) (Figure 4b) that is typical for V_2O_5 and mixed-valence vanadium oxides up to 350 °C.[9] Similar to vanadium(IV–V) oxides, the nanorods are mixed conductors where electrons[9] and oxygen vacancies[17,19] serve as the principal charge carriers. The H^+-hopping conductivity declared for vanadium pentoxide gels, $V_2O_5 \cdot nH_2O$, by Livage et al. was also observed and for the nanorods on the application of impedance spectroscopy.[20,21]

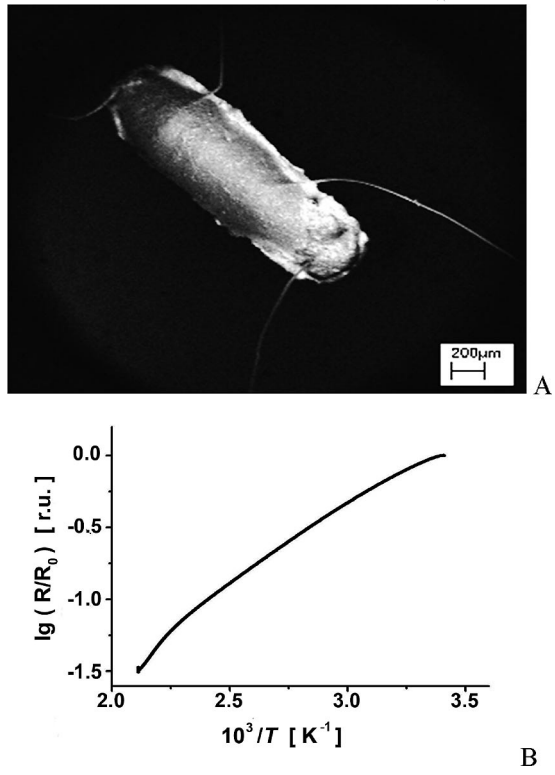

Figure 4. Micrograph of a two-probe chip for sensor properties examination (a). Temporal changes of resistivity with temperature during heating of vanadium oxide nanorods in air (b).

2.2. Synthesis of the Nanorods

Over the last decade, a number of research groups have reported new synthetic methods for vanadium oxide nanorods, nanobelts, and whiskers. For example, ref.[2] describes the preparation of nanorods of monoclinic bariandite $V_{10}O_{24} \cdot 12H_2O$ (PDF2 database file number 25-1006). In refs.[13,22] ribbon-like nanorods of monoclinic vanadium dioxide are reported. Whiskers of barium vanadium bronze based on a hydrated layered V_2O_5 structure have been reported recently.[23] In refs.[24,25] novel synthetic methods for $H_xV_2O_5 \cdot nH_2O$ nanorods are described.

By varying the concentration of ethanol in the reaction mixture, we found that both the microstructure and composition of the products obtained hydrothermally depend significantly on the composition and concentration of the organic additive; at low ethanol concentrations (less than 0.5 mol of C_2H_5OH to 1 mol of V_2O_5) the principal product was nanorods and at higher concentrations the preferred micromorphology of the product was nanoribbons and even nanosheets (Figure 6). The color of vanadium oxide also changes from light yellow to green and dark blue with varying ethanol concentration, demonstrating the increase in the percentage of V^{4+} in the product. According to XRD data, the desired $H_xV_2O_5 \cdot nH_2O$ nanorods were obtained only at low ethanol concentrations (V_2O_5/C_2H_5OH = 10:1), whereas at higher concentrations reduced vanadium oxides, such as $V_3O_7 \cdot H_2O$ (PDF2 database file number 28-1433)

and even monoclinic VO_2 (PDF2 database file number 71-42) were produced (Figure 6).

By varying the organic additives in the matrix solution we observed that hydroxy and carboxy groups led to the growth of 1D nanostructures. Mixtures with amine, thiol, sulfate, and azide groups assisted in the formation of different kinds of vanadium oxides, such as vanadium oxide nanotubes.[4]

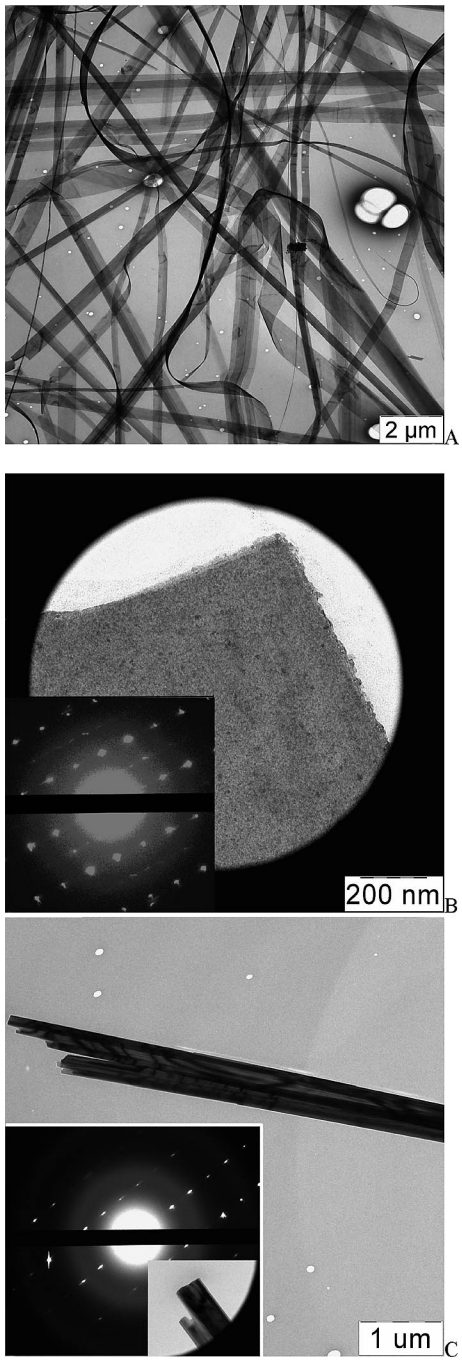

Figure 5. Micrographs of the products of hydrothermal treatment of V_2O_5/C_2H_5OH mixtures at different component ratios and autoclave infill levels (IL): (a) $H_xV_2O_5{\cdot}nH_2O$ nanoribbons (V_2O_5/C_2H_5OH = 4:1, IL 95%); (b) $V_2O_5{\cdot}nH_2O$ nanorods (V_2O_5/CH_3COOH = 4:1), IL 80%; (c) $V_2O_5{\cdot}nH_2O$ nanorods (nitric acid instead of ethanol, IL 80%).

Controlling the pressure during the synthesis by the infill level of the autoclave cell also changed the nature of the product. For instance, in case of low concentrations of ethanol (V_2O_5/C_2H_5OH = 10:1) an increase of the autoclave infill level up to 95% changed the micromorphology of the product, significantly intensifying the growth along the <010> axis and diminishing growth rates in the two other directions. The product of the synthesis was nanoribbons, about 20 μm in length, 50 nm in width, and only a few nm in thickness (Figure 5a). The oxidant–reductant interaction is also dependent on the infill level of the autoclave cell, which predetermines the V^{4+}/V^{5+} ratio in the product (Figures 5 and 6).

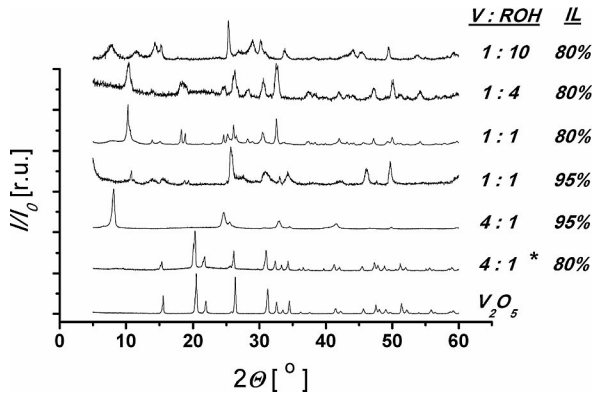

Figure 6. XRD data for vanadium oxide structures obtained in water/ethanol media at different infill levels of the autoclave cell and V_2O_5/C_2H_5OH ratios. Upwards: orthorhombic V_2O_5 (standard, precursor); $V_2O_5{\cdot}nH_2O$ nanorods (acetic acid instead of ethanol, IL 80%); $H_xV_2O_5{\cdot}nH_2O$ nanoribbons (ethanol, IL 95%); monoclinic VO_2 nanorods (ethanol, IL 95%); $V_3O_7{\cdot}nH_2O$ nanoribbons and nanosheets (2 patterns, ethanol, IL 80%); monoclinic VO_2 nanosheets (ethanol, IL 80%).

Initially, the role of the alcohol and hydroxy group derivatives in the nanorod formation mechanism was not clear. An excess of alcohol served as a reductant and prevented growth of the nanorods or nanoribbons resulting in monoclinic vanadium dioxide sheets or $V_3O_7{\cdot}H_2O$ nanoribbons (Figure 6). At the same time, the hydrothermal treatment of orthorhombic V_2O_5 at standard conditions resulted in the recrystallization of vanadia, but no nanorods are observed in the SEM and TEM micrographs.

The second role of the alcohol involves pH control. The presence of acetic acid in the matrix solution decreases the pH to 2–3, which is close to the electroneutrality of hydrolyzed vanadia species. According to ref.[26] an acidic medium produces vanadia frameworks built from layers of square pyramids or distorted octahedra. The hydrothermal treatment of V_2O_5 with acetic acid (V_2O_5/C_2H_5OH = 10:1) with an infill level of 80% resulted in the formation of light yellow vanadium pentoxide nanorods $V_2O_5{\cdot}nH_2O$ (about 60% yield) and greenish $H_xV_2O_5{\cdot}nH_2O$ nanorods (Figure 5b). The hydrothermal processing of V_2O_5 in the presence of dilute nitric acid HNO_3 (pH = 4) produces nanorods of $V_2O_5{\cdot}nH_2O$ (Figure 5c). The product was light yellow in color and, according to the XRD data, it was a textured orthorhombic V_2O_5 (PDF2 database file number 41-

1426); the yield of vanadia nanorods in this experiment did not exceed 30%. Such phenomena led us to suggest the role of V^{4+} to be important in the nucleation process and the pH to be significant for crystal growth.

Based on our observations, we assume that the growth mechanism for $H_xV_2O_5{\cdot}nH_2O$ nanorods, partly or completely, has to be similar to that of vanadia gel formation, in which the olation process is ruled by the pH.[17,25] Oxolation is also a pH-sensitive process and requires a pH of 2–3. Acetic acid, with its mild acidic nature, could serve as an acidic buffer ensuring optimal pH values during the synthesis.

2.3. Sensor Properties

Sensor characteristics of $H_xV_2O_5{\cdot}nH_2O$ nanorods for several gases are summarized in Table 1. The best sensitivities for most of the gases are at temperatures below 200 °C, because of the drastic increase in their conductivities with temperature. In most cases, the nanorods show reproducible behavior, i.e. their resistance reaches initial values as soon as the test gas is shut off (Figure 7).

Table 1. Sensor response (S) of powdery samples of nanorods to TEA, DMMP, CO, O_2, and NO_2 at different temperatures (T) and concentrations. Dried air served as the gas-carrier.

Species	T [°C]	Concentration	S [%]
O_2	120–180	0–20 vol.-%	chemisorption
NO_2	100–175	10 ppm	1–3
	200		1
TEA	125–175	10 ppm	4–25
	200	0.6 ppm	30
DMMP	200	0.6 ppm	no detection
CO	150–180	10 ppm	<0.3

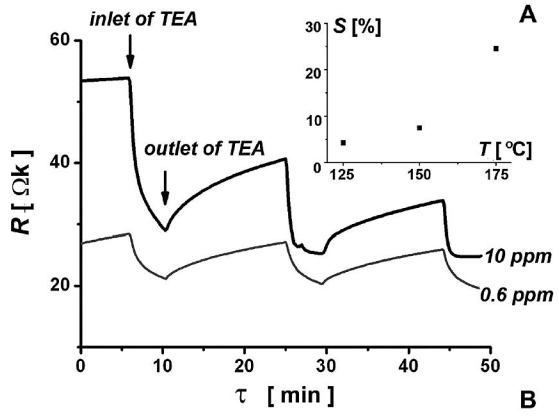

Figure 7. Concentration (a) and temperature (b) dependences of the sensor response in the presence of TEA for nanorods.

The influence of oxidizing agents on the specific resistance of the nanorods results in a conductivity decrease. The resistance of the sample was studied at 180, 150, and 120 °C in a variety of oxygen concentrations (see Experimental Section). It was found that the interaction of the nanorods with molecular oxygen is not reversible, because of the oxidation of vanadium(IV) at the nanorod surface; we have previously observed the same process for vanadium oxide nanotubes.[4] Above 150 °C the resistance of the material raises quickly and reaches a plateau.[27,28] The decrease of the oxygen concentration was detected at a permanent flow chromatographically and the resistance of the sample reached a plateau. The essential chemisorption of molecular oxygen by vanadia nanorods occurs only above 150 °C, then reaching a plateau with an equilibrium concentration.

The sensor response (S) of the nanorods to 10 ppm of triethylamine (TEA) was examined at different concentrations of the gas detected (Table 1, Figure 7). The S values are given in Figure 7b. It is evident that the adsorption–desorption processes are much more successful at 175 °C than at lower temperatures. The maximum point of the dome-shaped curve can be most likely found at higher temperatures, because of its tendency to growth. At 150 °C, the 75% sensor response (S_{75}) of vanadium oxide nanorods was achieved in 32 s, whereas the relaxation time (τ) was 5.5 min (Table 2). Presumably, the interaction of TEA molecules with the vanadia surface occurs mostly on the Lewis acid sites, which are not at all typical for hydrated V_2O_5.[19] Most likely, adsorption of TEA molecules occurs at Brønsted acid sites or $V^{5+}{}_{(5c)}$ and $V^{4+}{}_{(6c)}$ Lewis acid sites.[29] At the same time, in the case of vanadium pentoxide nanorods the obtained values of S are higher than for mixed-valence vanadium oxides.[24] Presumably, this originates from the higher conductance of mixed-valence vanadium oxides.

Table 2. Relaxation times τ_{75} for resistive-type gas sensors based on vanadium oxide nanorods in a 10 ppm TEA atmosphere.

T [°C]	τ_{75} [s]
175	32
150	40
125	110

The sensitivity of vanadium oxides to nitrogen dioxide is low because of the low chemical affinity of NO_2 molecules to V–O fragments (Table 1). The maximum S was found at about 175 °C. For this gas, S is less than 3%. This observation demonstrates reversible adsorption of NO_2 molecules that occurs over the temperature range, but the conductivity changes are negligible. This measurement was repeated after the experiments in TEA, and we observed the same character of S/T (temperature) dependence.

CO molecules cause no drastic changes in nanorod conduction (Table 1), and the CO adsorption is reversible. The maximum of sensitivity of vanadia nanorods to CO was found at 180 °C and is only 0.3%. At 150 °C, S is 0.1%. These response values are smaller than for polycrystalline orthorhombic V_2O_5 obtained elsewhere.[10]

Vanadium oxide nanorods are an interesting example of materials that demonstrate no sensitivity to poisonous dimethyl methylphosphonate (DMMP). It seems that vana-

dium pentoxide nanorods do not interact with either alkyl groups or the basic phosphorus site. Vanadium oxide nanorods may demonstrate some sensing activity to DMMP at temperatures higher than 200 °C.

In summary, we should underline that a response of the nanorods was detected only for TEA. The sensing properties of vanadium oxide nanorods are limited, most likely by the acidity of the surface. An interaction of TEA molecules with the vanadium oxide surface could be realized through Brønsted or Lewis acid sites. The presence of O–H groups at the nanorod surface was confirmed by XPS and FTIR data. Such sites are available for an unshared pair of TEA molecules. The other gases tested have no such properties and interact with the material weakly or not at all, giving small sensor responses.

3. Conclusion

Nanorods of $H_xV_2O_5{\cdot}nH_2O$ were hydrothermally obtained in water/ethanol and water/nitric acid environments and then tested as resistive-type gas sensor transducers. Vanadia nanorods have demonstrated a stable response to triethylamine under cycling and almost no sensor response to either carbon monoxide or nitrogen oxides. The reasons for such specificity of the sensor to amines are discussed in terms of particular adsorption and redox interaction of the amines with acidic sites of mixed-valence vanadium oxides. It is remarkable that the material shows no specificity to molecular oxygen and DMMP. This new material appears to be suitable for sensors working at relatively low temperatures.

Experimental Section

Vanadia nanorods were synthesized according to a standard hydrothermal treatment[24] of orthorhombic polycrystalline V_2O_5 (Sigma Aldrich) in aqueous media at 180 °C for 48 h by using a Teflon-lined capsule sealed in a steel autoclave. Ethanol and/or nitric acid (pure, Chimpromtorg) were added to obtain nanorods as the product. The product was repeatedly washed with an excess of distilled water and dried at 200 °C in air. The microstructure of the resulting product was examined with a transmission electron microscope (Leo 912 Omega AB, LaB_6 cathode, 100 kV) and a scanning electron microscope (LEO SUPRA 50VP, 5–25 kV) with an EDX analyzer (Inca, Oxford Instruments). XRD data were measured with a Rigaku D/MAX 2500 diffractometer (Japan) with a rotating copper anode (Cu-K_α) in a 2Θ range of 2–60° with a step of 0.02°. XPS data were measured with a LAS-3000 ("Riber") spectrometer with a semispherical analyzer OPX 150 with a retarding field. For the excitation of photoelectrons, Al-K_α (1486.6 eV) irradiation was applied (cathode ray tube voltage 12 kV, emission current 20 mA). Calibration of photoelectron peaks was performed against the 1s line of carbon with a binding energy of 285 eV. The surface area of the samples was calculated according to the BET method from nitrogen adsorption isotherms obtained with a Nova 4200e device (Quantachrome Instruments). Sensor properties of the nanorods were investigated in situ by using a special setup for resistive-type gas sensors tests. Measurements were performed at 200, 175, 150, 125, and 100 °C starting from the highest temperature. Prior to the measurements, the powder of vanadium oxide nanorods (about 12 mg) was mixed with α-terpineol ($C_{10}H_{17}OH$), which served as a binder. The paste was screen-printed onto a specially designed chip with four platinum contacts located on an alumina substrate (Figure 4b). The terpineol was burnt out by calcination at 200 °C. The gas effect on the electrical resistance was studied in a potentiostatic regime in a dynamic flow system with dry air as the carrier gas. The total flow rate was 100 mL/min. S was calculated as $S = (R_{max} - R_{min})/R_{min} \times 100\,\%$, where variables R_{max} and R_{min} are the sample resistances with and without an analyzing gas in artificially prepared mixtures; the sensitivity values were calculated as an average of five measurements.

Acknowledgments

The authors are grateful to Sergey S. Abramchuk (Lomonosov Moscow State University, Russia), Jennifer Haag (Ruhr-Universität Bochum, Germany), and Andrey B. Odintsov (Stanford University, USA) for their assistance in experiments and manuscript preparation. This work has been realized with financial support of the Russian Federal Agency on Science and Innovations and the Russian Foundation of Basic Research (project numbers 09-03-00602-a and 09-03-01122-a). This project is also supported by a grant from Haldør Topsoe A/S and the Deutscher Akademischer Austausch-Dienst (DAAD).

[1] F. Zhou, X. Zhao, C. Yuan, L. Li, *Cryst. Growth Des.* **2008**, *8*, 723–727.
[2] S. Pavasupree, Y. Suzuki, A. Kitiyanan, S. Pivsa-Art, S. Yoshikawa, *J. Solid State Chem.* **2005**, *178*, 2152–2158.
[3] C. Xiong, A. E. Aliev, B. Gnade, K. J. Balkus, *ACS Nano* **2007**, *2*, 293–301.
[4] A. V. Grigorieva, A. B. Tarasov, E. A. Goodilin, S. M. Badalyan, M. N. Rumyantseva, A. M. Gaskov, A. Birkner, Yu. D. Tretyakov, *Mendeleev Commun.* **2008**, *48*, 6–7.
[5] M. E. Spahr, P. Stoschitzki-Bitterli, R. Nesper, O. Haas, P. Novák, *J. Electrochem. Soc.* **1999**, *146*, 2780–2783.
[6] M. Niederberger, H.-J. Muhr, F. Krumeich, F. Bieri, D. Günther, R. Nesper, *Chem. Mater.* **2000**, *12*, 1995–2000.
[7] J. Liu, X. Wang, Q. Peng, Y. Li, *Adv. Mater.* **2005**, *17*, 764–767.
[8] N. Pinna, U. Wild, J. Urban, R. Schlogl, *Adv. Mater.* **2003**, *15*, 329–331.
[9] G. Eranna, B. C. Joshi, D. P. Runthala, R. P. Gupta, *Crit. Rev. Solid State Mater. Sci.* **2004**, *29*, 111–188.
[10] G. Micocci, A. Serra, A. Tepore, S. Capone, R. Rella, P. Siciliano, *J. Vac. Sci. Technol. A* **1997**, *15*, 34–38.
[11] N. Y. Shishkin, A. A. Komarov, D. V. Kosov, V. A. Cherkasov, L. A. Bashkirov, U. Bardi, Y. K. Gunko, *Sens. Actuators B* **2005**, *108*, 113–118.
[12] G. Gu, M. Schmid, P. W. Chiu, A. Minett, J. Fraysse, G. T. Kim, S. Roth, M. Kozlov, E. Munoz, R. H. Baughman, *Nat. Mater.* **2003**, *2*, 316–319.
[13] J. Dexmer, C. M. Leroy, L. Binet, V. Heresanu, P. Launois, N. Steunou, C. Coulon, J. Maquet, N. Brun, J. Livage, R. Backov, *Chem. Mater.* **2008**, *20*, 5541–5549.
[14] W. G. Menezes, D. M. Reis, M. M. Oliveira, J. F. Soares, A. J. G. Zarbin, *Chem. Phys. Lett.* **2007**, *445*, 293–296.
[15] P. Y. Zavalij, M. S. Whittingham, *Acta Crystallogr., Sect. B* **1999**, *55*, 627–663; C. Herwig, C. Limberg, *Inorg. Chem.* **2008**, *47*, 2937–2939.
[16] S. Surnev, M. G. Ramsey, F. P. Netzer, *Prog. Surf. Sci.* **2003**, *73*, 117–165.
[17] J. Livage, *Chem. Mater.* **1991**, *3*, 578–593.
[18] N. A. Chernova, M. Roppolo, A. C. Dillon, M. S. Whittingham, *J. Mater. Chem.* **2009**, *19*, 2526–2552.

[19] X. Yin, H. Han, I. Gunji, A. Endou, S. S. C. Ammal, M. Kubo, A. Miyamoto, *J. Phys. Chem. B* **1999**, *103*, 4701–4706.
[20] O. Schilling, W. Colbow, *Sens. Actuators, B* **1994**, *21*, 151–157.
[21] S. Kittaka, H. Hamaguchi, T. Shinno, T. Takenaka, *Langmuir* **1996**, *12*, 1078–1083.
[22] G. Andersson, *Acta Chem. Scand.* **1954**, *8*, 1599–1606.
[23] T. L. Kulova, A. M. Skundin, S. B. Balakhonov, D. A. Semenenko, E. A. Pomerantseva, A. G. Veresov, E. A. Goodilin, B. R. Churagulov, Yu. D. Tretyakov, *Prot. Met.* **2008**, *44*, 39–42.
[24] A. V. Grigorieva, E. A. Goodilin, A. V. Anikina, I. V. Kolesnik, Yu. D. Tretyakov, *Mendeleev Commun.* **2008**, *18*, 71–72.
[25] W. Avansi Jr., C. Ribeiro, E. R. Leite, V. R. Mastelaro, *Cryst. Growth Des.* **2009**, *9*, 3626–3631.
[26] P. Y. Zavalij, F. Zhang, M. S. Whittingham, *Acta Crystallogr., Sect. B* **1999**, *55*, 953–962.
[27] N. Barsan, U. Weimar, *J. Electroceram.* **2001**, *7*, 143–167.
[28] M. N. Rumyantseva, E. A. Makeeva, S. M. Badalyan, A. A. Zhukova, A. M. Gaskov, *Thin Solid Films* **2009**, *518*, 1283–1288.
[29] K.-I. Shimizu, I. Chinzey, H. Nishiyama, S. Kakimoto, S. Sugaya, W. Matsutani, A. Satsuma, *Sens. Actuators, B* **2009**, *141*, 410–416.

Received: May 26, 2010
Published Online: October 4, 2010

